# Synthesis and Redox Behavior of Flavin Mononucleotide-Functionalized Single-Walled Carbon Nanotubes

Sang-Yong Ju and Fotios Papadimitrakopoulos*

*Nanomaterials Optoelectronics Laboratory (NOEL), Polymer Program, Department of Chemistry, Institute of Materials Science, University of Connecticut, Storrs, Connecticut 06269-3136*

Received August 31, 2007;  E-mail: papadim@mail.ims.uconn.edu

***Abstract:*** In this contribution, we describe the synthesis and covalent attachment of an analogue of the flavin mononucleotide (FMN) cofactor onto carboxylic functionalities of single-walled carbon nanotubes (SWNTs). The synthesis of FMN derivative (**12**) was possible by coupling flavin H-phosphonate (**9**) with an aliphatic alcohol, using a previously unreported *N*-(3-dimethylaminopropyl)-*N*′-ethylcarbodiimide hydrochloride coupling. We found that the flavin moiety of **12**-SWNT shows a strong $\pi-\pi$ interaction with the nanotube side-walls. This leads to a collapsed FMN configuration that quenches flavin photoluminescence (PL). The treatment of **12**-SWNT with sodium dodecyl sulfate (SDS) overcomes this strong nanotube/ isoalloxazine interaction and restores the FMN into extended conformation that recovers its luminescence. In addition, redox cycling as well as extended sonication were proven capable to temporally restore PL as well. Cyclic voltammetry of FMN onto SWNT forests indicated profound differences for the extended and collapsed FMN configurations in relation to oxygenated nanotube functionalities that act as mediators. These findings provide a fundamental understanding for flavin-related SWNT nanostructures that could ultimately find a number of usages in nanotube-mediated biosensing devices.

## Introduction

Flavin is an important redox moiety for one- and two-electron-transfer cycles in cell membranes.[1,2] Scheme 1 illustrates a number of flavoprotein cofactors vital to cellular redox chemistry, such as riboflavin (Vitamin B$_2$, **2**) and flavin mononucleotide (FMN, **3**).[3] A number of applications have surfaced involving these cofactors in the presence or absence of apoproteins in the area of biosensors,[4,5] biocatalysis,[6] bioluminescence,[7,8] and biofuel cells.[9] Out of these flavin derivatives, FMN (**3**) is an important luciferin (i.e., bioluminescent cofactor) when reconstituted with apo-bacterial luciferase from *photobacterium fischeri*.[7,10,11] Upon introduction of an *n*-alkyl aldehyde and molecular oxygen substrates, the reduced holo-bacterial luciferase (containing FMNH$_2$) emits visible light at around 495 nm.[7]

**Scheme 1.** Chemical Structure of Isoalloxazine (**1**), Riboflavin (**2**), and Flavin Mononucleotide (FMN) (**3**)
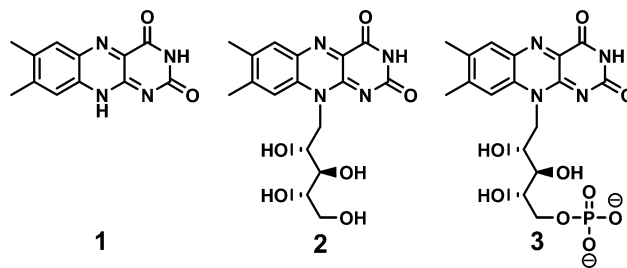


The unique electronic and electrochemical properties of single-walled carbon nanotubes (SWNTs) have inspired a number of biosensing methodologies for proteins,[12–14] DNA,[15] and aptamers,[16] using electrochemical- and transistor-based configurations. Flavin adenine dinucleotide (FAD) was shown to spontaneously adsorb onto nanotubes and facilitate quasi-reversible electron transfer with SWNT electrodes.[17] A recent theoretical study indicates that the flavin moiety of FAD forms strong $\pi-\pi$ interactions with both metallic and semiconducting

(1) Massey, V. *Biochem. Soc. Trans.* **2000**, *28*, 283−296.
(2) Stryer, L. *Biochemistry*, 4th ed.; W. H. Freeman & Company: New York, 1995.
(3) Walsh, C. *Acc. Chem. Res.* **1980**, *13*, 148−155.
(4) Willner, B.; Katz, E.; Willner, I. *Curr. Opin. Biotechnol.* **2006**, *17*, 589−596.
(5) Wang, J. *Electroanalysis* **2001**, *13*, 983−988.
(6) Niazov, T.; Baron, R.; Katz, E.; Lioubashevski, O.; Willner, I. *Proc. Natl. Acad. Sci. U.S.A.* **2006**, *103*, 17160−17163.
(7) Hastings, J. W. *Ann. Rev. Biochem.* **1968**, *37*, 597−630.
(8) Palomba, S.; Berovic, N.; Palmer, R. E. *Langmuir* **2006**, *22*, 5451−5454.
(9) Katz, E., Shipway, A. N., Willner, I., Eds. Biochemical fuel cells. In *Handbook of Fuel Cells: Fundamentals, Technology and Applications*; Wiley: 2003; Vol. 1, 1−27.
(10) Wilson, T.; Hastings, J. W. *Annu. Rev. Cell. Dev. Biol.* **1998**, *14*, 197−230.
(11) Meighen, E. A.; MacKenzie, R. E. *Biochemistry* **1973**, *12*, 1482−1491.

(12) Wang, J.; Liu, G.; Jan, M. R. *J. Am. Chem. Soc.* **2004**, *126*, 3010−3011.
(13) Yu, X.; Munge, B.; Patel, V.; Jensen, G.; Bhirde, A.; Gong, J. D.; Kim, S. N.; Gillespie, J.; Gutkind, J. S.; Papadimitrakopoulos, F.; Rusling, J. F. *J. Am. Chem. Soc.* **2006**, *128*, 11199−11205.
(14) Barisci, J. N.; Wallace, G. G.; Chattopadhyay, D.; Papadimitrakopoulos, F.; Baughman, R. H. *J. Electrochem. Soc.* **2003**, *150*, E409−E415.
(15) He, P.; Dai, L. *Chem. Commun.* **2004**, 348−349.
(16) So, H.-M.; Won, K.; Kim, Y. H.; Kim, B.-K.; Ryu, B. H.; Na, P. S.; Kim, H.; Lee, J.-O. *J. Am. Chem. Soc.* **2005**, *127*, 11906−11907.
(17) Guiseppi-Elie, A.; Lei, C.; Baughman, R. H. *Nanotechnology* **2002**, *13*, 559−564.

SWNTs.[18] In addition, the flavin adsorption energy onto SWNTs is an order of magnitude higher in strength (ca. 2 eV) than that of an equicyclic anthracene.[19]

The covalent attachment of redox cofactors onto a variety of conductive substrates (i.e., Au, nanotubes, etc.) has sparked considerable interest in mediatorless electrochemistry.[20,21] Patolsky et al. have realized the highest turnover rate to glucose oxidase (GOx) by the covalent attachment of FAD cofactor to the tips of SWNTs forests.[21] Such holoenzyme reconstruction could prove challenging for a side-wall grafted, flavin-containing cofactor, owing to the aforementioned strong $\pi-\pi$ attraction with the nanotube.

In this contribution we report the synthesis and covalent functionalization of a synthetic FMN cofactor (**12**) to carboxylic functionalized SWNTs. The synthetic design for this cofactor was based on a theoretical and experimental study indicating greater activity of bacterial luciferase than natural FMN.[11,22] To provide adequate distance between SWNT and FMN cofactor, an *n*-hexyl-spacer (toward CNT) and an *n*-pentyl spacer (toward flavin) on either sides of the phosphate group were introduced. A novel phosphite-assisted coupling methodology is also described based on *N*-(3-dimethylaminopropyl)-*N*′-ethylcarbodiimide hydrochloride (EDC). As expected, the flavin moiety of (**12**) strongly adheres to the side-walls of SWNTs, which quenches its luminescence. The detachment of the flavin cofactor from the side-walls of SWNTs was realized by treating with a surfactant (sodium dodecyl sulfate (SDS)) or by reducing the attached FMN to FMNH$_2$. These findings pave the way to ultimately link SWNTs with bacterial luciferase toward nano-structured bioluminescence devices, wherein the redox cycling of the flavin cofactor is electrically provided through the nanotube as opposed to the use of mediators.[23]

## Experimental

**Materials and Instrumentation.** All reagents were purchased from Sigma-Aldrich unless otherwise mentioned. All solvents were reagent grade. 5-Chloropentanol and D$_2$O (99.5%) were purchased from TCI and Acros, respectively. Precautions were taken to avoid prolonged exposure of isoalloxazine derivatives to direct sunlight and the blue/UV part of the visible spectra by performing the experiments in a laboratory lit with yellow fluorescent bulbs. Silica gel with 230−400 mesh was used for flash chromatography. Reverse phase C-18 columns (40 and 80 g purification capacity) was performed in a Companion flash chromatography apparatus (Teledyne Isco Inc.), equipped with a single-wavelength UV detector. Millipore quality deionized water with resistivity greater than 18 MΩ was used for all experiments. $^1$H, $^{13}$C, and $^{35}$P NMR spectra were acquired on an Avance spectrometer operating at a Larmor frequency of 300, 75, and 121.6 MHz, respectively, unless otherwise mentioned. All spectra were recorded in 5 mm NMR tubes containing 0.65 mL of DMSO-$d_6$ or D$_2$O at 295 K, unless otherwise mentioned. SWNTs, prepared by the high-pressure carbon monoxide (HiPco) chemical vapor deposition process,[24,25] were

obtained from Carbon Nanotechnologies, Inc. Fourier Transform Infrared (FTIR) spectra were obtained from a Nicolet Magna FTIR spectrometer using a HgGeTe detector (cooled or not cooled) at a spectral resolution of 4 cm$^{-1}$. KBr disks were used as supports and an incident angle of ca. 45° was used to minimize interference noise.[26] Room-temperature UV−vis−near IR absorption and photoluminescence (PL) spectra were obtained using a Perkin-Elmer LAMDA-900 UV−NIR spectrometer and a Perkin-Elmer LS50B Fluorometer, respectively. Atomic force microscopic (AFM) characterization was performed on a Topometrix Explorer and Asylum Research MFP-3D in contact mode and tapping mode, respectively. Cyclic voltammetry (CV) was measured using a CH Instruments 840B electrochemical workstation. Phosphate-buffer saline solution (PBS, pH 7.4, 0.1 M) was used as an electrolyte. The solution was rigorously purged with nitrogen prior to use, and all electrochemical data were recorded under a nitrogen atmosphere. A three electrode configuration was used with working electrodes made from either pyrolytic graphite (PG) or SWNT forests assembled on PG, a calomel reference electrode, and a platinum wire as a counter electrode.

**Synthesis. *N*-(5′-Hydroxypentyl)-3,4-dimethylaniline (5).** A mixture of 9.1 g (75 mmol) of 3,4-dimethylaniline (**4**) and 3.05 g (24.88 mmol) of 5-chloropentanol in 15 mL of triethylamine (TEA) was stirred at 110 °C for 6 h. After the mixture was cooled and methylenechloride (200 mL) was added, the organic solution was washed with aqueous Na$_2$CO$_3$ solution (10%, 40 mL). The aqueous layer was extracted twice with methylene chloride (2 × 100 mL). The combined organic extracts were dried over MgSO$_4$ and rotary evaporated to dryness. The thin-layer chromatography retention factor ($R_f$) of the target compound **5** was 0.1 with methylene chloride (MC)−methanol (MeOH) (95:5) and was confirmed by ninhydrin test. Compound **5** was purified by flash chromatography on silica gel in MC:MeOH (95:5) and crystallized from *n*-hexane to produce 4.1 g of white crystals (80% yield): mp 39−40 °C. $^1$H NMR (300 MHz, CDCl$_3$, Figure S1a of Supporting Information (SI)): δ 6.93 (1H, d, *J* = 8 Hz), 6.44 (1H, d, *J* < 2 Hz), 6.38 (1H, dd, *J* = 8, *J* < 2 Hz), 3.66 (2H, t), 3.10 (2H, t), 2.19 (3H, s), 2.15 (3H, s), 1.63 (4H, m), 1.47 (2H, m). $^{13}$C NMR (75 MHz, CDCl$_3$): δ 146.7, 137.5, 130.4, 125.5, 115, 110.6, 62.9, 44.5, 32.6, 29.5, 23.53, 20.2, 18.9. Anal. Calcd for C$_{13}$H$_{21}$NO (MW = 207.16): C, 75.32; H, 10.21; N, 6.76. Found: C, 74.92; H, 10.39; N, 6.65.

**6-[*N*-(5′-Hydroxypentyl)-3,4-xylidino] Uracil (6).** To a solution of compound **5** (2.9 g, 14 mmol) in water−dioxane (1:1; 30 mL) refluxed under argon, 0.672 g of 6-chlorouracil (4.59 mmol) was added with stirring. After 15 h of reflux, the solvent was removed, the residue was redissolved in water (40 mL), and the pH was increased to 11 by the addition of aqueous NaOH solution (10 w/v %). The resulting solution was extracted thrice with methylene chloride (3 × 70 mL) to remove unreacted starting compound **5**, which can be recycled. Aqueous HCl solution (38 wt. %) was added to reduce the pH of the aqueous extract down to pH 3, which induced precipitation of **6**. The resulting precipitate was collected by filtration and washed with water. Additional compound **6** was obtained from the filtrate after water evaporation, followed by dissolution in methanol, removal of undissolved moieties, and rotary evaporation of the methanol filtrate. Both fractions of **6** were combined and further purified by flash chromatography on a silica gel with MC/MeOH = 8:2 to recover 0.99 g (68% yield) of a yellow solid with bright blue luminescence in MeOH solution, mp 228 °C. $^1$H NMR (300 MHz, DMSO-$d_6$, Figure S1b of SI): δ 10.34 (1H, br s), 10.10 (1H, br s), 7.23 (1H, d, *J* = 4 Hz), 7.04 (1H, d, *J* < 2 Hz), 6.97 (1H, dd, *J* = 8, <2 Hz), 4.08 (1H, s), 3.57 (2H, t), 3.34 (2H, t), 2.24 (6H, s), 1.46 (2H, m), 1.38 (2H, m), 1.26 (2H, m). $^{13}$C NMR (75 MHz, DMSO-$d_6$): 164.1, 154.8, 151.7, 140.2, 138.5, 136.2, 131.2, 129.0, 125.4, 77.4, 61.0, 51.3, 32.6, 27.6, 22.8, 19.9, 19.44. Anal. Calcd for

(18) Lin, C. S.; Zhang, R. Q.; Niehaus, T. A.; Frauenheim, T. *J. Phys. Chem. C* **2007**, *111*, 4069−4073.

(19) Lu, J.; Nagase, S.; Zhang, X.; Wang, D.; Ni, M.; Maeda, Y.; Wakahara, T.; Nakahodo, T.; Tsuchiya, T.; Akasaka, T.; Gao, Z.; Yu, D.; Ye, H.; Mei, W. N.; Zhou, Y. *J. Am. Chem. Soc.* **2006**, *128*, 5114−5118.

(20) Xiao, Y.; Patolsky, F.; Katz, E.; Hainfeld, J. F.; Willner, I. *Science* **2003**, *299*, 1877−1881.

(21) Patolsky, F.; Weizmann, Y.; Willner, I. *Angew. Chem., Int. Ed.* **2004**, *43*, 2113−2117.

(22) Lin, L. Y.-C.; Sulea, T.; Szittner, R.; Vassilyev, V.; Purisima, E. O.; Meighen, E. A. *Protein Sci.* **2001**, *10*, 1563−1571.

(23) Karatani, H.; Konaka, T. *Bioelectrochem. Bioenerg.* **1998**, *46*, 227−235.

(24) Nikolaev, P.; Bronikowski, M. J.; Bradley, R. K.; Rohmund, F.; Colbert, D. T.; Smith, K. A.; Smalley, R. E. *Chem. Phys. Lett.* **1999**, *313*, 91−97.

(25) Bronikowski, M. J.; Willis, P. A.; Colbert, D. T.; Smith, K. A.; Smalley, R. E. *J. Vac. Sci. Technol. A* **2001**, *19*, 1800−1805.

(26) Papadimitrakopoulos, F.; Konstadinidis, K.; Miller, T. M.; Opila, R.; Chandross, E. A.; Galvin, M. E. *Chem. Mater.* **1994**, *6*, 1563−1568.

$C_{17}H_{23}N_3O_3 \cdot 0.6H_2O$ (MW = 328.20): C, 62.21; H, 7.43; N, 12.80. Found: C, 62.14; H, 7.33; N, 12.69.

**Isoalloxazine 5-Oxide (7).** Sodium nitrite (0.35 g, 5.14 mmol) was added to a solution of compound **6** (0.35 g, 1.1 mmol) in acetic acid (5 mL) in a dark environment. The mixture was stirred at room temperature for 3 h, and 2 mL of water was subsequently added. The suspension was stirred for 3 h prior to rotary evaporation out of all solvents. Compound **7** was obtained by filtration after the addition of 5 mL of ethanol and brief sonication. This was recrystallized from acetic acid or ethanol to produce 0.3 g of **7** (80% yield), mp 228 °C, dec. ^{1}H NMR (500 MHz, DMSO-$d_6$, Figure S1c of SI): $\delta$ 11.02 (1H, s), 8.09 (1H, s), 7.79 (1H, s), 4.52 (2H, t), 4.40 (1H, t), 3.44 (2H, q), 2.48 (3H, s), 2.39 (3H, s), 1.72 (2H, m), 1.50 (4H, m). ^{13}C NMR (125 MHz, DMSO-$d_6$): 157.2, 155.1, 153.1, 147.1, 136.1, 133.0, 132.5, 125.4, 120.4, 117.5, 61.1, 44.5, 32.7, 27.0, 23.2, 20.6, 19.4. Anal. Calcd for $C_{17}H_{20}N_4O_4 \cdot 0.5H_2O$ (MW = 353.38): C, 57.78; H, 5.99; N, 15.85. Found: C, 57.41; H, 5.83; N, 15.55.

**N-(5'-Hydroxypentyl) Isoalloxazine (8).** An aqueous solution of dithiothreitol (DTT, 1.4 g, 3.18 mmol, 7 mL of water) was added to a suspension of **7** (0.25 g, 0.66 mmol) in ethanol (200 mL). The mixture was refluxed under argon for 4 h. After the solution became clear, the organic solvent was evaporated, and the residue was soaked with 5 mL of ethanol and filtered. The yellowish-orange solid was recrystallized from ethanol to provide 0.23 g of **8** (96% yield), mp 293 °C, followed with subsequent decomposition. ^{1}H NMR (500 MHz, DMSO-$d_6$, Figure S1d of SI): $\delta$ 11.28 (1H, br s), 7.90 (1H, s), 7.79 (1H, s), 4.58 (2H, br t, J = 7 Hz), 4.40 (1H, t, J = 5 Hz), 3.43 (2H, q), 2.52 (3H, s), 2.41 (3H, s), 1.73 (2H, m), 1.50 (4H, m); ^{13}C NMR (125 MHz, DMSO-$d_6$): 160.4, 156.1, 150.5, 147.0, 137.6, 136.2, 134.3, 131.5, 131.2, 116.5, 61.024, 44.67, 32.65, 26.87, 23.32, 21.08, 19.3. Anal. Calcd for $C_{17}H_{20}N_4O_3 \cdot 0.3H_2O$ (MW = 333.78): C, 61.17; H, 6.22; N, 16.79. Found: C, 61.46; H, 6.23; N, 16.46.

**Flavin Pentyl *H*-Phosphonates (9).** Compound **8** (52.54 mg, 0.16 mmol) was dissolved in dry pyridine (10 mL) at 100 °C under argon in a dark environment. The solution was subsequently cooled to 30 °C, and phosphorous acid (54 mg, 0.66 mmol) was added prior to the addition of 97 mg (0.32 mmol) of 2,4,6-triisopropylbenzenesulfonyl chloride. The mixture was stirred at room temperature for 15 h, and the solvent was evaporated. The residue was purified by flash chromatography either on a reverse C-18 column (40 g cartridge, Teledyne ISCO) in water or on a silica gel in MC—MeOH gradient (which takes significantly longer than the reverse C-18 column) to yield compound **9**. In the case of using reverse phase C-18 column, **9** comes out together with pyridine and water, both of which need to be removed by washing with ethanol. The final yellow solid was obtained with a yield of 80% (mixture of acid and its pyridinium salt (1:2 ratio, as inferred by the ^{1}H NMR of Figure S1e)), mp 175 °C, followed with subsequent decomposition. ^{1}H NMR (300 MHz, DMSO-$d_6$, Figure S1e of SI): $\delta$ 11.31 (1H, br s), 8.71 (1.5H, pyridine, d, J = 4 Hz), 8.1 (0.75H, pyridine, t, J = 7 Hz), 7.84 (1H, s), 7.77 (1H, s), 6.72 (1H, d, $J_{P-H}$ = 665 Hz), 4.55 (2H, br t), 3.91 (2H, br q), 2.50 (3H, s), 2.38 (3H, s), 1.69 (4H, m), 1.52 (2H, m). ^{13}C NMR (75 MHz, DMSO-$d_6$): 160.4, 156.2, 150.4, 147.2, 140.4, 137.5, 136.3, 134.2, 131.4, 131.1, 125.6, 116.5, 64.23, 44.5, 30.1, 26.44, 22.85, 21.0, 19.3. ^{31}P NMR (121.5 MHz, 85% $H_3PO_4$ as a external reference, $D_2O$): 9.66 (1H, d, $J_{HP}$ = 660 Hz). Anal. Calcd for $C_{17}H_{21}N_4O_5P \cdot 1.6H_2O$ (MW = 421.18): C, 48.48; H, 5.79; N, 13.30; P, 7.35. Found: C, 48.27; H, 5.59; N, 12.94; P, 7.11.

**(6-Hydroxy-hexyl)-carbamic Acid *tert*-Butyl Ester (HHCar).** To a mixture of di-*tert*-butyl dicarbonate (11 g, 50 mmol) in methanol (100 mL), 6-amino hexyl alcohol (5.8 g, 49.5 mmol) dissolved in methanol (200 mL) was added dropwise. The solution was stirred overnight at room temperature, and the methanol was removed away by rotary evaporation. The resulting solid was extracted with methylene chloride against water. The organic layer was evaporated, and the residue was purified using flash chromatography on a silica gel column

from a gradient of methylene chloride/methanol with a gradual increase of methanol to produce 9.6 g of **HHCar** (89% yield), a waxy solid, mp 35—36 °C, followed with subsequent decomposition. ^{1}H NMR (300 MHz, DMSO-$d_6$, Figure S1i of SI): $\delta$ 6.75 (1H, br t), 4.33 (1H, t), 3.37 (2H, q), 2.88 (2H, q), 1.37 (13H, m), 1.26 (4H, m). ^{13}C NMR (75 MHz, DMSO-$d_6$): 156.0, 77.7, 61.1 33.0, 30.0, 28.7, 26.7, 25.7. Anal. Calcd for $C_{11}H_{23}NO_3$ (MW = 217.17): C, 60.80; H, 10.67; N, 6.45. Found: C, 60.99; H, 10.90; N, 6.88.

**(6-([Flavin-pentyloxy]-*H*-phosphoryl)-hexyl)-carbamic Acid *tert*-Butyl Ester (10).** Compound **9** (0.284 g, 0.72 mmol) was dissolved in dry pyridine (100 mL) at 100 °C under argon in dark environment and cooled to 30 °C prior to adding **HHCar** (0.315 mg, 1.45 mmol) and *N*-(3-dimethylaminopropyl)-*N'*-ethylcarbodiimide hydrochloride (EDC, 0.6 g, 2.9 mmol). The mixture was stirred for 24 h and the resulting organic solvents were removed via rotary evaporation. TLC indicated a new spot (i.e., compound **10**) with $R_f$ = 0.45 using methylenechloride/ methanol (9:1). Compound **10** was purified by chromatography on silica gel in methylene chloride—methanol (95:5) (0.263 g, 78%): mp 131 °C, followed with subsequent decomposition. ^{1}H NMR (300 MHz, DMSO-$d_6$, Figure S1f of SI): 11.3 (1H, br s), 7.91 (1H, s), 7.81 (1H, s), 6.82 (1H, d, $J_{P-H}$ = 693 Hz), 6.76 (1H, br t), 4.59 (2H, br t), 4.0 (4H, m), 2.89 (2H, q), 2.51 (3H, s), 2.41 (3H, s), 1.71 (4H, m), 1.56 (4H, m), 1.36 (9H, s), 1.26 (6H, m). ^{13}C NMR (75 MHz, DMSO-$d_6$): 160.4, 156.1, 156.0, 150.5, 147.1, 137.5, 136.2, 134.2, 131.5, 131.1, 116.5, 77.7, 65.5,65.4, 65.3, 65.2, 49.1, 44.4, 30.3, 30.2, 30.0, 29.8, 28.7, 26.4, 26.2, 25.1, 22.7, 21.0, 19.2. ^{31}P NMR (121.5 MHz, 85% $H_3PO_4$ as a external reference, [1]H-decoupled, $D_2O$): 16.58, 10.87 ($J^1_{P-H}$ = 660 Hz, d, $J^3_{P-H}$ = 2.4 Hz, quintet). Anal. Calcd for $C_{28}H_{42}N_5O_7P \cdot CH_3$-OH (MW = 623.67): C, 55.85; H, 7.43; N, 11.23; P, 4.97. Found: C, 56.63; H, 7.48; N, 11.27; P, 4.75.

**(6-([Flavin-pentyloxy]-phosphoryloxy)-hexyl)-carbamic Acid *tert*-Butyl Ester (11).** Compound **10** (84 mg, 0.142 mmol) was dissolved in 0.2 M iodine in pyridine—THF (1:1, 10 mL) in a dark environment and triethylamine (1 mL) was added. The mixture was stirred for 5 h, and then water was added. TLC showed a new spot with $R_f$ = 0 (i.e., compound **11**) using MC/MeOH (9:1), whereas the rest of starting reagents have higher $R_f$. The resulting organic solution was evaporated, and the resulting residue was purified with a reverse phase C-18 column (80 g pack, Teledyne ISCO) using water—MeOH gradient (starting from 100:0 and finishing at 50:50) to produce 40 mg of **11** (46% yield), mp 120 °C, followed with subsequent decomposition. ^{1}H NMR (300 MHz, DMSO-$d_6$, Figure S1 g of SI): 11.31 (1H, br s), 7.87 (1H, s), 7.81 (1H, s), 6.76 (1H, br t), 3.62 (4H, m), 2.85 (2H, m), 2.51 (3H, s), 2.38 (3H, s), 1.72 (2H, m), 1.40—1.65 (6H, m), 1.34 (9H, s), 1.23 (6H, m). ^{13}C NMR (75 MHz, DMSO-$d_6$): 160.4, 156.2, 156.0, 150.4, 147.2, 137.1, 136.2, 134.2, 131.5, 131.2, 116.54, 77.7, 64.3, 56.5, 31.0, 30.9, 30.7, 30.0, 26.8, 25.7, 23.3, 21.0, 19.3. ^{31}P NMR (121.5 MHz, 85% $H_3PO_4$ as a external reference, $D_2O$): −1.10 (1H, s).

**6-([Flavin-pentyloxy]-phosphoryloxy)-hexyl-ammonium-tri-fluroro Acetic Acid Salt (12).** Trifluoroacetic acid (1 mL) was added to a solution of compound **11** (36 mg, 0.0593 mmol) in methylene chloride (10 mL). The mixture was rapidly stirred at room temperature for 30 min, and the organic solvent was completely evaporated. The resulting residue was purified using reverse C-18 column (80 g pack, Teledyne Isco Inc.) using water—MeOH gradient (starting from 100:0 and ending to 0:100) as eluent to produce 35 mg of **12** (95% yield), mp 120 °C. ^{1}H NMR (300 MHz, DMSO-$d_6$, Figure S1h of SI): 7.58 (1H, s), 7.54 (1H, s), 4.52 (2H, br t), 3.76 (2H, q), 3.69 (2H, q), 2.87 (2H, t), 2.43 (3H, s), 2.30 (3H, s), 1.75 (2H, m), 1.62 (2H, m), 1.35—1.6 (6H, m), 1.23 (4H, m). ^{13}C NMR (75 MHz, DMSO-$d_6$): 160.5, 158.6, 156.2, 147.2, 137.6, 136.3, 134.3, 131.5, 131.2, 116.6, 66.1, 44.2, 44.5, 30.1, 30.0, 27.3, 26.6, 25.7, 25.0, 22.8, 21.1, 19.3. ^{31}P NMR (121.5 MHz, 85% $H_3PO_4$ as a external reference, $D_2O$): −1.49 (1H, s).

**Acid Functionalization of SWNTs (a-SWNTs).** A 100 mg portion of HiPco SWNTs (Lot. CM26-0036AB-1) was shortened and carboxylic

**Scheme 2.** Synthetic Route for Realizing Amine-Terminated Analogues of FMN[a]
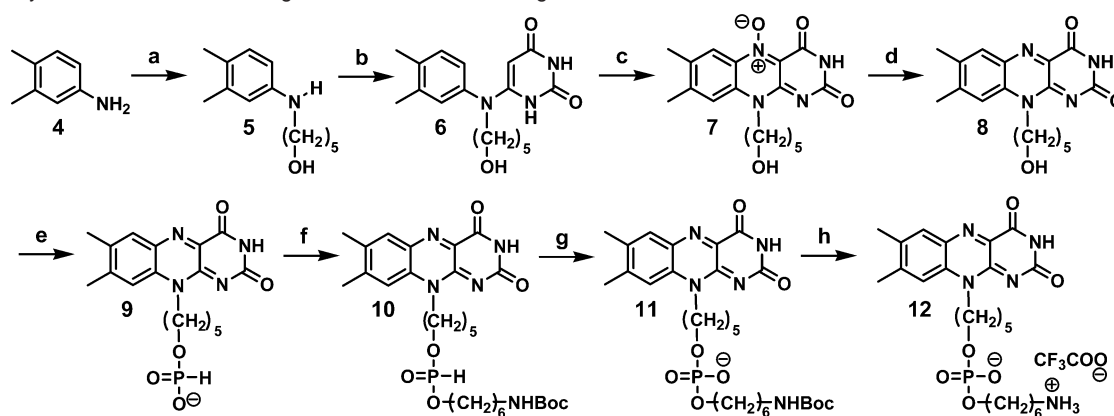


[a] Conditions: (a) $HO(CH_2)_5Cl/TEA$, reflux; (b) 6-chlorouracil/$H_2O$/dioxane, reflux; (c) $NaNO_2$/AcOH, room temp; (d) DTT/EtOH, reflux; (e) $H_3PO_3$/$TPSO_2Cl$/Py, room temp; (f) $HO(CH_2)_6NH$-*t*-BOC/EDC/Py, room temp; (g) $I_2$/THF/Py, room temp followed by $H_2O$ addition; (h) triflic acid/$CH_2Cl_2$, room temp.

functionalized by sonication-assisted oxidation in 40 mL of a 3/1 v/v mixture of $H_2SO_4$ (96.4%) and $HNO_3$ (98%), on the basis of a previously established method.[27,28] The resulting black solution was mildly sonicated for 4 h prior to filtering it from a 0.45 $\mu$m Teflon filter. The precipitate was washed with copious amount of water until the pH of the filtrate reached 6, and then it was vacuum-dried at 60 °C for 1 day to provide **a**-SWNTs.

**Coupling 12 with a-SWNTs and Purification (12-SWNT).** A 5 mg portion of **a**-SWNT was dispersed in DMF (20 mL) using mild sonication (80 W) for 1 h. To this 5 mg (8 $\mu$mol) of **12** and 20 mg (100 $\mu$mol) of EDC were added, and the mixture was stirred overnight. After adding 50 mL of acetone to the mixture to facilitate precipitation of the **12-**SWNT adduct, the flocculate was filtered and washed with copious amount of water and then dried in vacuum. A 3 mg portion of **12-**SWNT was redispersed in 10 mL of deionized (DI) water and mildly sonicated (80 W, Cole Parmer 8891) for 10 min to generate a greenish-gray homogeneous suspension of **12-**SWNT and physisorbed **12**. Subjecting this suspension to a 10 min, 5000*g* centrifugation resulted in precipitating out the **12-**SWNT adduct while leaving behind a bright greenish supernatant solution of **12** that was easily decanted. This sonication−centrifugation−decantation cycle was repeated four times to remove the noncovalently coupled **12** from the SWNTs.

**Dispersion of 12-SWNT Using Sodium Dodecyl Sulfate (SDS).** A 0.5 mg portion of **12-**SWNT (or **a**-SWNT) was mildly sonicated (80 W) in 4 mL of DI water containing 1 wt. % of SDS, according to a previously described methodology.[29]

**Redox Cycling of 12-SWNT.** A mixture of 1 mg of **12-**SWNT in 4 mL of $D_2O$ was suspensioned for 20 min using a cup−horn sonication (Cole Parmer ultrasonicprocessor) at 600 W intensity. The resulting suspension was subjected to two sonication−centrifugation−decantation cycles described above, prior to taking the supernatant. The suspension was then purged with Argon (99.998%, oxygen level around few ppm) in a capped cuvette and purged for 20 min prior to collecting both UV−vis−NIR and PL spectra. Following the addition of an adequate amount of a 1 M of sodium dithionite ($Na_2S_2O_4$) $D_2O$ solution, the **12-**SWNT $D_2O$ suspension (with or without SDS) was purged with Ar for an additional 10 min prior to collecting both UV−vis−NIR and PL spectra. Similar redox cycling was performed with **8** as the model compound.

**Covalent Attachment of 12 onto SWNT Forests.** SWNT forests on pyrolytic graphite (PG) electrode were prepared according to literature.[30] In brief, polished PG electrodes were immersed in 90% v/v methanolic solution of Nafion (5 wt. %, Sigma-Aldrich) for 15 min, followed by washing with water. Subsequently, these electrodes were immersed in aqueous iron(III) chloride solution (5 mg/mL) for 15 min, followed by washing the excess of $FeCl_3$ in DMF before immersing it in a DMF dispersion of **a**-SWNT (ca. 0.1 mg/mL) for 30 min, to facilitate the vertical nanotube forest assembly.[13,30,31] These nanotube forest (NTF)-modified electrodes were rinsed with copious amounts of methanol, dried and covalently functionalized by reacting **12** (2 mM) with carboxyl moiety of the NTF in the presence of EDC (20 mM), and dissolved in 50 $\mu$L of water for 3 h.[13] These electrodes were then rinsed with copious amounts of water and dried in air.

## Results and Discussion

The multiplicity of hydroxyl groups in natural flavin mono-nucleotide (FMN) (**3**), renders challenging the controllable covalent attachment of **3** to carboxyl-functionalized SWNTs (**a**-SWNTs). This directed us to investigate hydroxyl-lacking FMN derivatives that possess similar cofactor activity with luciferase.[11,22] As explained in the Introduction section, the phosphate derivative of **8** (see Scheme 2) does meet this requirement, and its synthesis has been previously reported by Frier et al.[32] The introduction of a *n*-pentyl, as opposed to *n*-hexyl spacer between the isoalloxazine ring (**1**) and phosphate group was found to provide a much higher binding affinity toward apo-luciferase.[11] Steps a−e in Scheme 2 illustrate the previously established methodology for the synthesis of the H-phosphite derivative of **8**, which upon $I_2$-assisted oxidation produces the phosphate derivative of **8**. Further functionalization of the *n*-hexyl H-phosphite derivative has been also reported using adamantine carboxylic acid chloride activation to attach this to the 3′-end of DNA oligomers. As will become apparent later on in the discussion, the adamantine carboxylic acid chloride activation is unsuitable for realizing a phosphodiester derivative of **9**. In this contribution, a versatile coupling methodology has been developed using EDC to link an *N*-protected aminoalcohol with the H-phosphite group (Scheme

(27) Liu, J.; Rinzler, A. G.; Dai, H.; Hafner, J. H.; Bradley, R. K.; Boul, P. J.; Lu, A.; Iverson, T.; Shelimov, K.; Huffman, C. B.; Rodriguez-Macias, F.; Shon, Y.-S.; Lee, T. R.; Colbert, D. T.; Smalley, R. E. *Science* **1998**, *280*, 1253−1256.
(28) Chattopadhyay, D.; Galeska, I.; Papadimitrakopoulos, F. *J. Am. Chem. Soc.* **2003**, *125*, 3370−3375.
(29) O'Connell, M. J.; Bachilo, S. M.; Huffman, C. B.; Moore, V. C.; Strano, M. S.; Haroz, E. H.; Rialon, K. L.; Boul, P. J.; Noon, W. H.; Kittrell, C.; Ma, J.; Hauge, R. H.; Weisman, R. B.; Smalley, R. E. *Science* **2002**, *297*, 593−596.

(30) Yu, X.; Kim, S. N.; Papadimitrakopoulos, F.; Rusling, J. F. *Mol. BioSyst.* **2005**, *1*, 70−78.
(31) Wei, H.; Kim, S. N.; Marcus, H. L.; Papadimitrakopoulos, F. *Chem. Mater.* **2006**, *18*, 1100−1106.
(32) Frier, C.; Decout, J.-L.; Fontecave, M. *J. Org. Chem.* **1997**, *62*, 3520−3528.

2f). Upon $I_2$ oxidation and amine deprotection, the *n*-pentyl-FMN cofactor **12** was covalently coupled to the carboxyl functionalities of **a**-SWNTs.

The synthetic steps that lead to the synthesis of **9** are listed in Scheme 2 and were reproduced from a previous report.[32] To provide adequate distance between a carbon nanotube and the phosphate group of the FMN cofactor, while ensuring electron tunneling from the nanotube to isoalloxazine moiety, HO-$(CH_2)_6$-$NH_2$ was chosen as an FMN−SWNT spacer. For this, the *N*-*t*-Boc protected aminohexylalcohol (**HHCar**) was first synthesized, as described in the Experimental section. The coupling of **HHCar** to **9** was proven unsuccessful using adamantine carboxylic acid chloride activation of the H-phosphite group of **9**. While the production of adamantine carboxylic ester of **9** was confirmed by TLC, this compound was proven quite stable against subsequent displacement by **HHCar**.

An alternative methodology to link **HHCar** to **8** and produce compound **11** was also attempted using the *N,N*-diisopropyl-chloro phosphoramidite and proved unsuccessful on the basis of the extreme $O_2$ and light susceptibility of the intermediate that quickly returned to the phosphate derivative of **8**.[32] For this, a new coupling methodology has been developed using carbodiimide chemistry, such as EDC.

EDC is well-known coupling agent for amide formation between carboxylic acids and amine groups[33] or phosphoramide formation between phosphate and amine groups.[34] To the best of our knowledge, EDC has never been used for the coupling of a hydroxyl group on H-phosphite with primary alcohols. Compound **9** was first dissolved in pyridine at 100 °C, and the clear solution was cooled to room temperature to avoid possible deprotection of the *t*-Boc group of **HHCar**. Subsequently, **HHCar** and excess of EDC ( 2 equiv of limiting reagent) were added and stirred for 24 h to afford a yield of 78% (Scheme 2f). Here, it is worth mentioning that the pyridine used in this coupling was reagent grade and not dried, unlike the two aforementioned coupling methodologies.[32,35] Compound **9** can be regenerated if EDC is not used in excess to remove the residual water in pyridine, thereby lowering the yield. As presented in the Experimental section, $^1H$, $^{13}C$, and $^{31}P$ liquid NMR, as well as elemental analysis has been used to confirm the formation of **10**. The $^{31}P$ NMR of **9**, **10**, **11**, and **12** will be further discussed below. The more acidic nature of hydroxyl group of phosphite group, as compared to carboxylic acid, is currently believed to be responsible for the efficient coupling of H-phosphite with the primary hydroxyl group.

Following the successful formation of **10**, the H-phosphite diester was oxidized using $I_2$ in the presence of pyridine to afford compound **11** with a yield of 46%. This was followed by amine group deprotection using trifluoroacetic acid, while the phosphordiester linkage remains intact. Figure 1 illustrates the $^{31}P$ NMR of compounds **9**−**12**. Spectra were obtained with and without proton decoupling to confirm the local environment of the phosphorus atom.[36] With the proton decoupler on, the $^{31}P$ NMR of compound **9** and $H_3PO_3$ (internal standard) produced a singlet
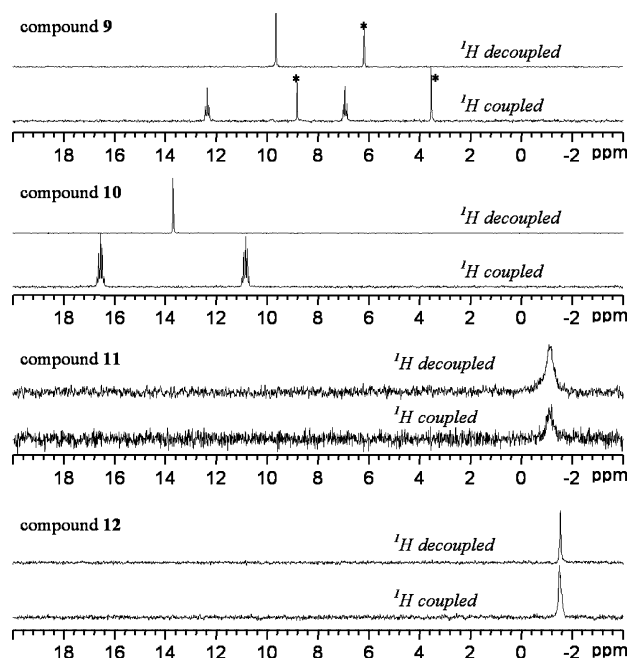
**Figure 1.** $^{31}P$ NMR of compounds **9**−**12** in $D_2O$. $H_3PO_3$ was used as internal standard for only compound **9** and is indicated with a star. The indicated $^{31}P$ NMR shifts were against $H_3PO_4$ as an external standard.

around 9.66 and 6.18 ppm,[36] respectively, against $H_3PO_4$ as an external standard. When the proton decoupler was off ($^1H$ coupled), the phosphite proton of **9** was split into two triplets centered around 12.39 and 6.95 ppm, respectively, with short-range coupling of phosphite proton to $^{31}P$ at $J^1_{P-H} = 660$ Hz. Such triplet splitting ($J^3_{P-H} = 8.92$ Hz) originates from the neighboring −O−$CH_2$− group, while the acidic nature of the P−OH proton renders it highly exchangeable with deuterium from the $D_2O$ solvent and therefore does not participate in this splitting. Similar short-range coupling was observed for the $H_3$-$PO_3$ (H−PO−$(OH)_2$) of the internal standard, with no further long-range coupling. For **10**, the presence of two neighboring −O−$CH_2$− groups produce shift the $^{31}P$ peak to 13.7 ppm (with the proton decoupler on). When the proton decoupler was turned off, two quintets were produced with a short- and long-range coupling from the phosphite and methylene protons, respectively, centered at 16.6 and 10.9 ppm, ($J^1_{P-H} = 693$ Hz and $J^3_{P-H} = 7.43$ Hz). In the case of compound **11**, the lack of phosphite $^1H$ resulted in single $^{31}P$ peak (ca. −1.10 ppm) for both the proton decoupler on and off. The poor signal-to-noise ratio along with the two remote −O−$CH_2$− groups renders unresolvable the $^1H$ long-range coupling when the decoupler was off. Compound **12** showed a similar $^{31}P$ position (ca. −1.49 ppm) with **11**, while this time the higher signal-to-noise ratio revealed a poorly resolved quintet with significant line broadening, when the proton decoupler was off.

Following the successful synthesis and characterization of **12**, its amine moiety was EDC-coupled with the carboxylic acid groups on SWNTs (**12**-SWNT). This was realized by dispersing **a**-SWNTs in DMF, subsequently adding **12** in the presence of EDC, and allowing the mixture to stir overnight (Scheme 3). Since the flavin moiety was shown to strongly adsorb onto SWNTs,[17,18] extensive sonication−centrifugation−decantation (SCD) cycles (at least four times using 10 min bath sonication at 80 W intensity) were required to completely remove physisorbed **12** moieties on SWNTs, while leaving behind the

(33) Sheehan, J. C.; Ledis, S. L. *J. Am. Chem. Soc.* **1973**, *95*, 875−879.
(34) Adessi, C.; Matton, G.; Ayala, G.; Turcatti, G.; Mermod, J. J.; Mayer, P.; Kawashima, E. *Nucleic Acids Res.* **2000**, *28*, E87.
(35) Usman, N.; Ogilvie, K. K.; Jiang, M. Y.; Cedergren, R. J. *J. Am. Chem. Soc.* **1987**, *109*, 7845−7854.
(36) Gorenstein, D. G. *Phosphorus-31 NMR: Principles and Applications*, 1st ed.; Academic Press: Orlando, FL, 1984.
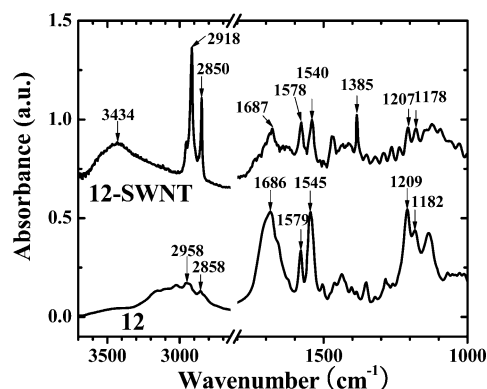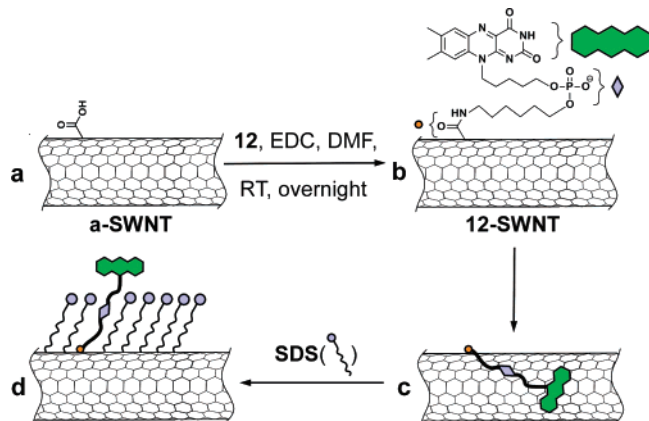
**Figure 2.** FTIR spectra of **12**-SWNT (top), and **12** (bottom).

**Scheme 3.** Covalent Attachment of **12** to Acid-Treated SWNTs (a,b) and Flavin-Tethered SWNTs and Its Conformation in the Absence (c) and Presence (d) of Sodium Dodecylsulfate (SDS)
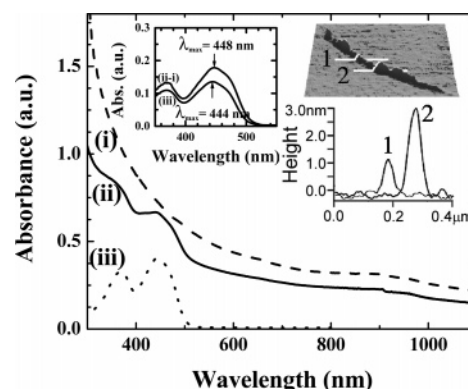




**Figure 3.** UV−vis−NIR spectra of SDS-dispersion of **a**-SWNT (i, dashed line), **12**-SWNT (ii, solid line), and **12** (iii, dotted line). Left inset shows the spectral subtraction of ii − i as compared to iii, while the two right insets depict AFM traces and line profiles of **12**-SWNT on mica.

covalently grafted adduct of **12**. The complete removal of residual physisorbed **12** was confirmed using $^1$H NMR with 98% deuterated SDS-$d_{25}$ surfactant (see Figure S2 in Supporting Information). In the case of physisorbed **12** on SWNT, treatment with SDS-$d_{25}$ was intended to disperse SWNTs in $D_2O$ and to liberate any residual **12** that can be easily detected from its aromatic region of $^1$H that persisted in the four SCD cycles. As proven by Figure S2, no residual **12** was detected, indicating that the four SCD cycles were sufficient to completely remove the physisorbed **12** from **12**-SWNT adduct.

Figure 2 illustrates the FTIR of **12**-SWNT and **12**. The increase in the broad 3450 cm$^{-1}$ N−H stretching vibration from **12** to **12**-SWNT is in accordance with the formation of an amide group on top of the uracil N−H of the isoalloxazine ring.[37] This is in agreement with the simultaneous decrease of the broad N−H stretching of the RNH$_3^+$ salt of **12** (ranging from 3300−2600 cm$^{-1}$) in the **12**-SWNT spectrum during the formation of the amide linkage. While the amide-I band overlaps with the already existing amide linkages from the isoalloxazine ring, an increase is witnessed for the 1578 cm$^{-1}$ (amide-II) mode as compared to the 1540 cm$^{-1}$ C=N out-of-plane stretching mode of flavin moiety or the 1209 and 1182 cm$^{-1}$ absorptions of the phosphate diester group.[37] The pronounced increase of the 1385 cm$^{-1}$ absorption in **12**-SWNT as compared to **12** is presently unknown. However, this peak might originate from the N$_1$−C$_2$−N$_3$ antisymmetric stretching accompanied by the deformation of the uracil moiety of the isoalloxazine group and might

be enhanced because of the strong flavin adsorption onto the side-walls of the SWNTs.[37] Such strong absorption of the flavin moiety on the SWNTs is expected to also lead to a conformational collapse of the FMN onto the side-wall of the nanotube (see Scheme 3c). The asymmetric and symmetric C−H stretching bands at 2917 and 2856 cm$^{-1}$, respectively, provide an initial indication for such collapsed conformation. Unlike the broad and weak 2958 and 2858 cm$^{-1}$ C−H stretching in **12**, the sharp 2918 and 2850 cm$^{-1}$ C−H stretching in **12**-SWNT indicates an entirely different −(CH$_2$)− conformation in either case.[38,39] On comparison with linear paraffin C$_n$H$_{2n+2}$ evaporated on gold, one can conclude that the alkyl groups of **12** are packed irregularly in its salt form.[38,39] Once **12** is coupled on the SWNTs, the pronounced increase in C−H stretching intensity suggests a substantial ordering of the alkyl spacers at the vicinity of the nanotubes. This might originate from favorable hydrophobic interactions with the highly ordered graphene side-walls of SWNTs.[38,39] This is schematically illustrated at the bottom right part of Scheme 3, which is synergistic with the facile adsorption of the flavin moiety onto SWNTs. Such adsorption will also force the hydrophilic phosphate diester in the vicinity of the nanotube. As will become evident later on in the discussion, such a configuration renders **12**-SWNT dispersible in aqueous media, yet quenches the strong photoluminescence efficiency of the isoalloxazine ring (**1**).

Figure 3 illustrates the UV−vis spectra of aqueous dispersions of **a**-SWNTs (i) and **12**-SWNTs (ii), in comparison to an aqueous solution of **12** (iii). In excess of four successive sonication−centrifugation decantation cycles have been applied to **12**-SWNT to ensure that only covalently linked FMN groups remain onto the SWNTs. The lack of sharp E$_{22}$ and E$_{11}$ absorptions, at 600−1000 and 1000−1600 nm ranges, respectively, are indicative of the substantial side-wall oxidation and/or the presence of small bundles of SWNTs. The two pronounced peaks of iii at 371 and 444 nm are characteristic of the isoalloxazine ring. The top-left inset of Figure 3 illustrates the spectral subtraction of i from ii, in comparison to iii. The close spectral resemblance of this subtracted peak (ii − i) to iii provides an additional confirmation for the successful attachment of **12** to SWNTs. Upon closer inspection, however, a 4 nm red-

(37) Abe, M.; Kyogoku, Y. *Spectrochim. Acta* **1987**, *43A*, 1027−1037.

(38) Porter, M. D.; Bright, T. B.; Allara, D. L.; Chidsey, C. E. D. *J. Am. Chem. Soc.* **1987**, *109*, 3559−3568.

(39) Nuzzo, R. G.; Fusco, F. A.; Allara, D. L. *J. Am. Chem. Soc.* **1987**, *109*, 2358−2368.
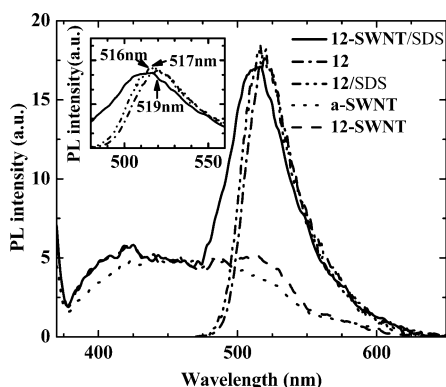
**Figure 4.** Solutions PL spectra of various constructs. Inset illustrates a close up at 520 nm. Excitation wavelength was 350 nm.

shift is observed for the $\lambda_{max}$ of (ii − i)) (448 nm) as opposed to the $\lambda_{max}$ of iii (444 nm). This slight red-shift might originate from the strong physisorbtion of flavin onto SWNTs (as indicated by both experimental[17] and theoretical studies[18]). A recent report on DNA-wrapped nanotubes also indicates similar red-shifts due to $\pi-\pi$ stacking of both purine and pyrimidine bases.[40] While $\pi-\pi$ stacking is known to produce slight hypochromism,[40] one can utilize the flavin extinction coefficient at the 444 nm absorption peak (12600 L/mol·cm)[32] to make a rough estimate of the % of covalent functionalization of FMN on SWNTs. Since not all SWNTs get suspended, and a significant fraction remains as a precipitate, the amount of suspended nanotubes was estimated by the extinction coefficient reported for acid-treated HiPco SWNTs at 9750 cm$^{-1}$ (1025 nm) in terms of carbon equivalency (260 ± 20 L/mol·cm).[41] On the basis of these two values, the covalent functionalization of **12**-SWNT was estimated to one FMN residue for every 43– 50 carbons. This value is in good agreement with the percent carboxylic acid functionalization on the SWNT, as introduced by the specific acid treatment.[42]

The upper right inset of Figure 3 illustrates a representative tapping-mode height AFM-image of **12**-SWNT deposited on mica substrate. The line-scans along positions 1 and 2 are shown below. The approximate height of SWNTs produced by the HiPco synthesis methodology is on the order of 1 nm,[43] which is in good agreement with the indicated height of line-scan 1. A number of protruding features can be seen distributed unevenly along this nanotube with height varying from 2 to 3 nm, believed to originate from the attached FMN groups.

**Photoluminescence Behavior.** Figure 4 illustrates the 350 nm excited photoluminescence (PL) spectra of **12**, SDS-dispersed **12** (**12**/SDS), and SDS-dispersed **12**-SWNT (**12**-SWNT/SDS), normalized with respect to their maximum intensity at ca. 517 nm. In addition, the PL spectra of **12**-SWNT and **a**-SWNT are also plotted and normalized at the 460 nm with respect to the absorption of **12**-SWNT/SDS sample. **12** emits brightly at green, with an emission maxima of 519 in dilute (10$^{-4}$ M and below) water solutions, which is the characteristic emission of the flavin moiety (see Figure S3 of

the Supporting Information). On the other hand, the as-synthesized **12**-SWNT showed almost no flavin-originated PL, with an exception of a shoulder at ca. 520 nm, situated on top of a broad emission feature (370−600 nm) of **a**-SWNTs. This broad **a**-SWNT PL emission is believed to originate from a variety of carbonaceous fragments during acid-purification procedure of SWNTs.[44] The $\pi-\pi$ stacking between the isoalloxazine ring and the side-walls of SWNTs[17,18] appears to be responsible for such quenching, as shown in Scheme 3c. Similar PL quenching has been reported for pyrene,[45−47] and metalloporphyrin derivative,[48] onto the sidewalls of SWNTs. The sonication-assisted dispersion of **12**-SWNT with sodium dodecyl sulfate (SDS) (0.1 w/v %) is capable of recovering the flavin luminescence, as shown in Figure 4. Such PL recovery originates from the effective micellerization of SWNTs by SDS that organize tightly along the nanotube side-walls and prevent readsorption of the flavin moiety to SWNT. This is schematically illustrated in Scheme 3d.

Upon closer inspection of the PL emission of **12**, **12**/SDS, and **12**-SWNT/SDS one can witness a progressive broadening of their PL full-width-half-maximum (FWHM) from 42 to 48 and 63 nm as well as a gradual blue-shift of the PL peak emission from 519 to 517 and 516 nm, respectively. Such blue-shift is believed to originate by lowering of the dielectric constant of the surrounding media from water to the aliphatic SDS tail group.[49] Similarly, the progressive broadening of fwhm demonstrates the inhomogeneity that the flavin moiety experiences in the proximity of SDS and SDS/SWNT.

**Chemical Redox Behavior.** The redox properties of the flavin group are of profound importance to biocatalysis.[6] Figure 5 illustrates the UV−vis and PL behavior of **8** as a function of its redox state. Initially, the aqueous solution of **8** was purged with argon for 20 min to completely remove any dissolved O$_2$. Subsequently, two aliquots of aqueous solution of dithionite (Na$_2$S$_2$O$_4$) (3.3 × 10$^{-4}$ M each) was added sequentially to 9 × 10$^{-6}$ M of **8** to reduce the oxidized form of flavin to the reduced form,[1,11] as shown in Scheme 4, and its UV−vis and PL (350 nm excitation) were collected prior to the addition of the next dithionite aliquot. Next, 100 mL of air (9.3 × 10$^{-4}$ M of O$_2$) was slowly bubbled to the solution of dithionite and **8**, to return back the flavin to its original oxidation state.[1] Such reduction is associated with luminescence quenching and a profound conformational change for the isoalloxazine ring away from planarity, as can be witnessed from Scheme 4.[50,51] This redox cycle is also accompanied by major changes in the UV−vis spectra of **8**, as shown in Figure 5. The oxidized and reduced forms of **8** have their first absorption maximums at 444 and 316 nm, indicative of the presence and lack of extended

(40) Hughes, M. E.; Brandin, E.; Golovchenko, J. A. *Nano Lett.* **2007**, *7*, 1191– 1194.
(41) Zhao, B.; Itkis, M. E.; Niyogi, S.; Hu, H.; Zhang, J.; Haddon, R. C. *J. Phys. Chem. B* **2004**, *108*, 8136–8141.
(42) Marshall, M. W.; Popa-Nita, S.; Shapter, J. G. *Carbon* **2006**, *44*, 1137– 1141.
(43) Fantini, C.; Jorio, A.; Souza, M.; Strano, M. S.; Dresselhaus, M. S.; Pimenta, M. A. *Phys. Rev. Lett.* **2004**, *93*, 147406.

(44) Xu, X.; Ray, R.; Gu, Y.; Ploehn Harry, J.; Gearheart, L.; Raker, K.; Scrivens, W. A. *J. Am. Chem. Soc.* **2004**, *126*, 12736–12737.
(45) Alvaro, M.; Atienzar, P.; Bourdelande, J. L.; Garcia, H. *Chem. Phys. Lett.* **2004**, *384*, 119–123.
(46) Liu, L.; Wang, T.; Li, J.; Guo, Z.-X.; Dai, L.; Zhang, D.; Zhu, D. *Chem. Phys. Lett.* **2002**, *367*, 747–752.
(47) Qu, L.; Martin, R. B.; Huang, W.; Fu, K.; Zweifel, D.; Lin, Y.; Sun, Y.-P.; Bunker, C. E.; Harruff, B. A.; Gord, J. R.; Allard, L. F. *J. Chem. Phys.* **2002**, *117*, 8089–8094.
(48) Murakami, H.; Nomura, T.; Nakashima, N. *Chem. Phys. Lett.* **2003**, *378*, 481–485.
(49) Greaves, M. D.; Deans, R.; Galow, T. H.; Rotello, V. M. *Chem. Commun.* **1999**, 785–786.
(50) Zhang, W.; Zhang, M.; Zhu, W.; Zhou, Y.; Wanduragala, S.; Rewinkel, D.; Tanner, J. J.; Becker, D. F. *Biochemistry* **2007**, *46*, 483–491.
(51) Dixon, D. A.; Lindner, D. L.; Branchaud, B.; Lipscomb, W. N. *Biochemistry* **1979**, *18*, 5770–5775.
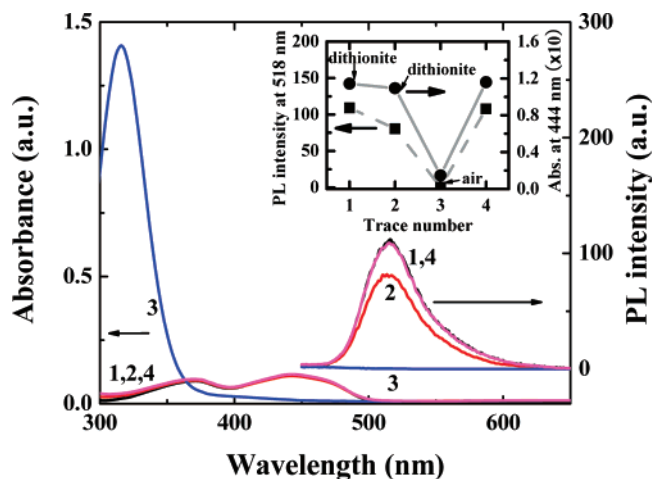
**Figure 5.** UV−vis (left) and PL (right) spectra of **8** ($9 \times 10^{-6}$ M) (trace 1) upon sequential sodium dithionite reduction (traces 2 and 3, for $3.3 \times 10^{-4}$ M $Na_2S_2O_4$ added each) and air ($O_2$) reoxidation (trace 4, $9.3 \times 10^{-4}$ M $O_2$ added), respectively. Inset shows tracewise changes of PL (left) and UV−vis absorption (right) at 518 and 444 nm, respectively. Lines were added to guide the eye. Excitation wavelength was 350 nm.

**Scheme 4.** Chemical Structure and Side View of Molecular Conformation of Flavin in Its Oxidized (left) and Reduced (right) State, along with Its Luminescence Characteristics
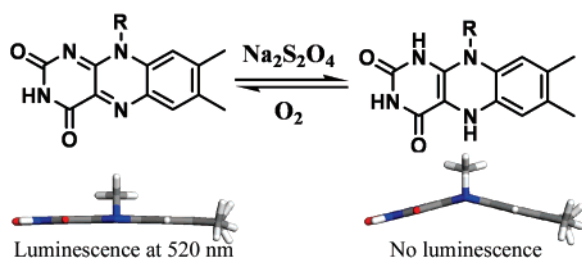


π-conjugation in the isoalloxazine ring, respectively. The dithionite reduction and $O_2$-assisted reoxidation is traced in the inset of Figure 5 by tracking both the 444 and 519 nm UV−vis absorption and PL emission, respectively. The addition of two aliquots of dithionite was found capable to completely convert **8** to its reduced form (trace #3).[50,51] The fully reversible redox of **8** was demonstrated by the addition of an excess amount of molecular oxygen that returns the flavin moiety back to its oxidized form (trace #4). Compounds **8**−**12** exhibited similar reversible redox behavior in terms of their absorption and PL characteristics that helped us establish an important control toward the investigation of the redox properties of **12**-SWNT.

Figure 6 panels A and B illustrate the redox-dependent changes of the 444 nm UV−vis absorption and 520 nm PL emission of **12**-SWNT in the absence and presence of SDS, respectively (as obtained from Figure S4 of the Supporting Information). Since the as-synthesized **12**-SWNT exhibits little or no PL emission at 516−520 nm because of the strong π−π interactions of flavin with SWNTs, intense sonication treatment was required to temporarily detach the tethered flavin moiety from the nanotube side-walls. Upon addition of one aliquot of dithionite, all covalently attached flavin moieties were transformed to their reduced form (in the presence or absence of SDS), since the flavin concentration onto **12**-SWNT ($5.8 \times 10^{-7}$ M) was substantially lower that that of dithionite ($9 \times 10^{-6}$ M). Subsequently, two additions of 3 and 15 mL of air ($2.8 \times 10^{-5}$ and $1.4 \times 10^{-4}$ M of $O_2$) were added, respectively, shown in trace no. 3 and no. 4. In the absence of SDS (Figure 6A),
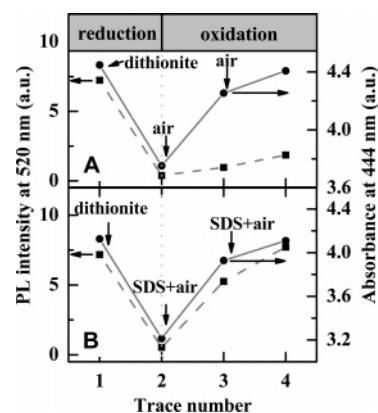


**Figure 6.** Tracewise changes of PL (left) and UV−vis absorption (right) at 520 and 444 nm, respectively of **12**-SWNT, upon sequential addition of $Na_2S_2O_4$ (reduction) and air ($O_2$) (oxidation), in the absence (A) and presence (B) of SDS. Lines were added to guide the eye. Excitation wavelength was 350 nm.

while the UV−vis absorption of **12**-SWNT at 444 nm was completely restored, after the second air addition, the PL emission recovered only by ca. 30%. Subsequent addition of air did not increase the PL emission from the 30% level. On the other hand, in the presence of SDS, the PL emission recovered completely (trace no. 3 and no. 4 of Figure 6B). This provides an additional indication that in the absence of SDS nanotube coating, the strong π−π interactions of the reoxidized FMN promote a collapsed configuration of the flavin on the nanotube side-walls as shown in Scheme 3c.

**Electrochemical Studies of Flavin Derivatives on SWNT Forests Arrays.** The electrochemical response of redox reagents greatly depends on their ability to rapidly diffuse to and from the working electrode. While this is the case for small molecules, the large hydrodynamic volume of **12**-SWNT profoundly impedes the aforementioned diffusion. To overcome this problem, the redox behavior of covalently and noncovalently attached flavin moieties was studied on top of SWNT forest arrays.[17,21] These vertically aligned arrays of nanotubes provide good electrical contacts with the underlying electrode, as well as the necessary carboxylic functionalities for covalent attachments of **12**. A large number of studies have shown that such forest configuration provides approximately an order of magnitude enhancement in signal-to-noise ratio that has been instrumental for development of ultrasensitive electrochemical sensors.[13,30,52] While the exact nature of such enhancement is not completely elucidated, it is strongly believed that is related to the presence of oxygenated sites (i.e., phenols and corresponding quinones) at the tips of these nanotube forests.[53] These oxygenated sites provide effective mediation in the vicinity of these tips, which are responsible for obtaining an ideal separation between oxidation and reduction peaks at 25 °C (i.e., $59/n$ mV, where $n$ is the number of electrons per molecule).[53] The only drawback of these nanotube forest (NTF) electrodes is their susceptibility to sonication, which disassembles such forest assembly. This prevents the use of sonication for desorbing the flavin moiety from nanotubes, thereby limiting us only to redox-assisted desorption (described above).

Figure 7 illustrates the cyclic voltamograms (CVs) of two flavin derivatives **8** and **12** in the presence and absence of SDS.

(52) Yu, X.; Chattopadhyay, D.; Galeska, I.; Papadimitrakopoulos, F.; Rusling, J. F. *Electrochem. Commun.* **2003**, *5*, 408−411.
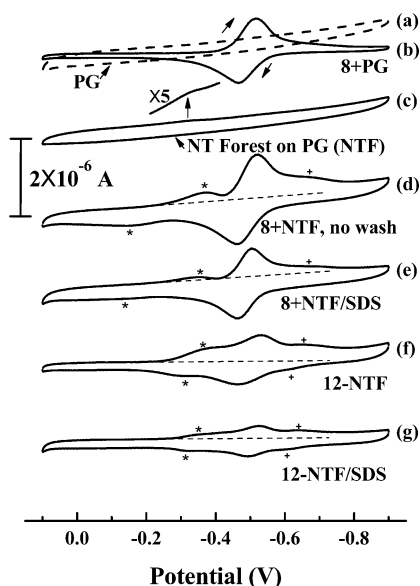(53) Gooding, J. J. *Electrochim. Acta* **2005**, *50*, 3049−3060.

**Figure 7.** Cyclic voltamograms obtained from a different electrode in PBS (pH 7.4, 0.1 M). Each CV was offset by $2 \times 10^{-6}$ A. Scan rate was 50 mV/s.

In addition, the CVs of PG and NTF on PG working electrodes are provided as controls (Figure 7a,c). These CVs were recorded in a phosphate buffer saline (PBS) solution in the absence of oxygen to prevent unwanted oxygen reduction of ca. −0.6 V. Both PG and NTF working electrodes show featureless CVs from 0.1 to −0.9 V versus calomel reference electrode. Upon closer inspection (5× magnification), the bare NTF electrode shows a minute anodic hump around −0.3 V which is believed to originate from the oxygenated functionalities (i.e., phenolic/quinoid moieties) at the tips of the severed, acid-purified carbon nanotubes.[52]

Figure 7 panels b and d illustrate the CVs of the dilute ($5 \times 10^{-5}$ M) solution of **8** in PBS, in the absence and presence of the nanotube forest (NTF). In the absence of NTF, **8** shows a reversible redox wave centered ca. −0.49 V, separated by 50 mV.[21] The anodic wave peaking at −0.52 V has been assigned to the sequential two-electron flavin reduction, which along with two-proton addition, transforms FMN to $FMNH_2$.[54] In the presence of NTF, two additional reduction peaks (−0.37 and −0.67 V) are witnessed in the anodic wave, marked with a star and a cross, respectively. In the cathodic wave, an additional oxidation peak is witnessed at ca. −0.15 V, marked with a star. The peak separation between the oxidation and reduction peaks marked with stars is ca. 220 mV. On the basis of such redox peak separation, the corresponding oxidation peak of the cross-marked anodic wave at −0.67 V should overlap with the main cathodic wave of **8** (−0.47 V, see Figure 7b,d). To investigate the nature of these two additional redox waves, extensive washing with PBS of the **8**+NTF electrode was performed, and its CV was obtained in PBS in the absence of **8**. (see Figure S5 of the Supporting Information). Much to our surprise, a significant signal was observed, although the majority of **8** should have been washed away. Two broadened waves are visible (cathodic/anodic at −0.51/−0.35 V (marked with stars) and −0.64 and −0.47 V (marked with crosses)), both separated by ca. 160 mV. These two waves are believed to originate from

physisorbed flavins, whose strong interaction with the nanotube side-walls has been demonstrated by Guiseppi-Elie et al.[17] Such a strong $\pi-\pi$ interaction might split the combined two-electron reduction of FMN to $FMNH_2$ into two separate waves, for reasons that are not currently known. The equal spacing (ca. 160 mV) between anodic and cathodic peaks for both waves appear to support such hypothesis. While the second redox wave (marked with +) of Figure S5 coincides with that of Figure 7d, the first redox wave (marked with ∗) is shifted by 170 mV toward a higher negative potential. Such a shift might originate from the fact that the physisorbed flavin moieties are expected to physisorb stronger to the stems, as opposed to the oxygenated tips of the SWNT forests, where stable $\pi-\pi$ interaction with the pristine graphene side-walls of SWNT can prevent their desorption from multiple PBS washing. Correspondingly, the separation of such stem-physisorbed flavin moieties from the mediation-prone oxygenated tips of SWNT forests could account for the aforementioned −170 mV shift of the first redox wave.

Figure 7e illustrates the comparable CV of Figure 7d, only this time SDS was added along with **8**. While all three waves maintained their redox-potential positions, a generic reduction in current intensity was observed for all waves. Since SDS is known to physisorb on nanotubes,[55] such current reduction appears to originate from the insulating properties of SDS.

Figure 7 panels f and g illustrate the CVs of **12** covalently attached on the tips of SWNT forests in the absence and presence of SDS, respectively. Considerable washing and redox cycling was performed to ensure that no unreacted **12** remains in the vicinity of forests. The most striking feature of Figure 7f,g as compared to Figure 7d,e is that covalent functionalization resulted in the narrowing of peak separation for both star and cross waves (from 160 to ca. 40−50 mV). This enabled the reappearance of the cathodic peak of the wave marked with the cross, which led further credence to the assignment of the marked waves to physisorbed FMN. Such dramatic narrowing is believed to originate from the effective mediation that the oxygenated forest tips provide to the attached **12** on these tips. The relative magnitude of redox activity (amperometric current) from Figure 7d to 7f illustrates the profound electrochemical activity of covalently attached FMN onto SWNTs. However, the relative magnitude of the star and cross-peaks (corresponding to physisorbed FMN) in Figure 7f are twice as large as that of Figure 7d. This is in direct agreement with the aforementioned tendency of **12** to adopt a collapsed configuration onto SWNTs. While the insulative nature of SDS lowers the magnitude of all three redox waves, the star and cross waves (attributed to collapsed **12**) appeared to be impacted at greater extent, which is in accordance with the chemical redox behavior of **12**-SWNT, observed spectroscopically.

## Conclusions

In this contribution, the covalent functionalization of SWNTs with flavin mononucleotide (FMN) is reported. This functionalization was realized via a novel EDC-assisted coupling of an H-phosphite derivative of FMN (**9**) to an alcohol-terminated spacer, containing an amine-protected moiety on its other end. Upon oxidation of the phosphite group to phosphate and subsequent amine-deprotection, the FMN derivative of (**12**) was

(54) Cooke, G.; Duclairoir, F. M. A.; John, P.; Polwart, N.; Rotello, V. M. *Chem. Commun.* **2003**, 2468−2469.

(55) Richard, C.; Balavoine, F.; Schultz, P.; Ebbesen, T. W.; Mioskowski, C. *Science* **2003**, *300*, 775−778.

covalently attached to acid-functionalized SWNTs via EDC coupling (**12**-SWNT). The strong $\pi-\pi$ interaction of aromatic flavin moiety causes a collapsed FMN configuration onto the side-walls of SWNTs that quenches its fluorescence. The detachment of flavin moiety can be temporally achieved by either sonication or chemical reduction of FMN to $FMNH_2$ and reoxidation back to the fluorescent FMN state. The micellerization of the SWNT with sodium dodecyl sulfate (SDS) surfactant was proven to be an effective way to prevent the long-term collapse of FMN onto the SWNTs. Fluorescence and UV–vis absorption spectroscopy, in conjunction with cyclic voltammetry (CV) were utilized to characterize the redox behavior of **12**-SWNT, in comparison to a nanotube-unbound FMN derivative (**8**). The dithionite- and $O_2$-assisted reduction and reoxidation to $FMNH_2$ and FMN, respectively, was quantitatively achieved as long as the flavin moieties did not exhibit a collapsed conformation onto the nanotube side-walls. The CV of **12** attached to the tips of SWNT forests showed that the redox behavior of extended and collapsed FMN is significantly impacted by the presence of oxygenated moieties, which act as mediators. These findings establish a basic understanding in terms of synthesis and redox-assisted conformational behavior of covalently bound SWNT FMN derivatives toward the ultimate goal of incorporating them into functional bioelectronic devices.

**Supporting Information Available:** ^{1}H NMR spectra for compounds **5**−**12**, **HHCar**, and **12**-SWNT (encapsulated in perdeuterated SDS micelles); UV−vis and PL spectra of compounds **8**−**12** and **12**-SWNT in the presence and absence of SDS while exposed to dithionite and air ($O_2$), respectively; the CV of physisorbed **8** onto SWNT forests is. This material is available free of charge via the Internet at http://pubs.acs.org.

JA076598T

# Synthesis and Redox Behavior of FMN Functionalized Single-Walled Carbon Nanotubes
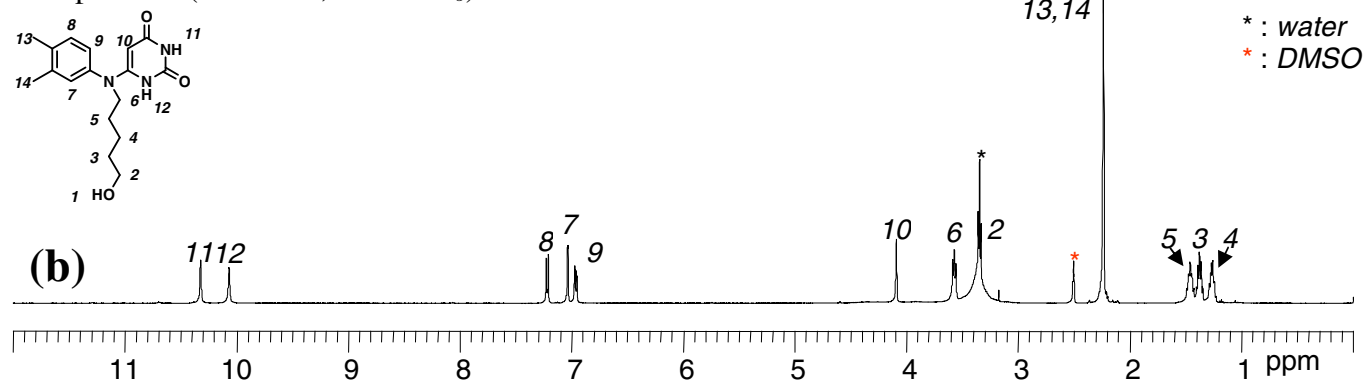
Sang-Yong Ju and Fotios Papadimitrakopoulos[*]

Contribution from the Nanomaterials Optoelectronics Laboratory (NOEL), Polymer Program,

Department of Chemistry, Institute of Materials Science, University of Connecticut, Storrs, Connecticut

06269-3136

**Figure S1**. ^{1}H NMR spectra of compounds **5 – 12** and **HHCar**.
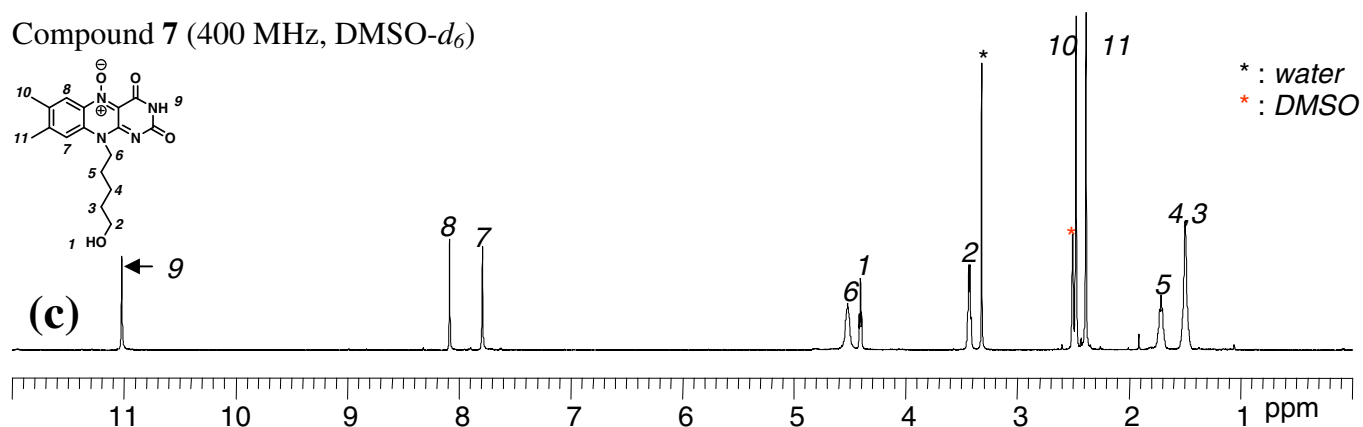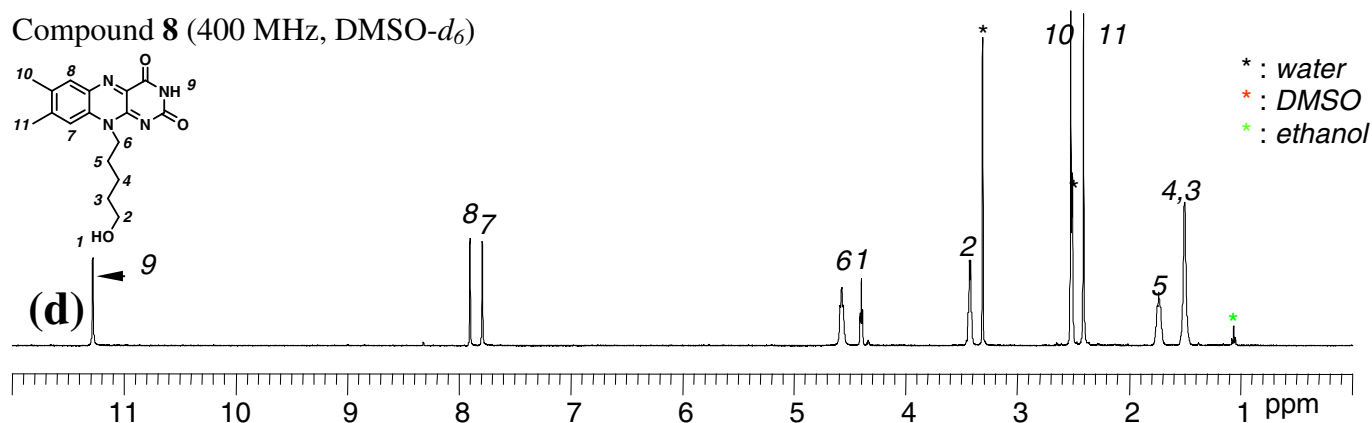
Compound **5** (300MHz, CDCl$_3$)
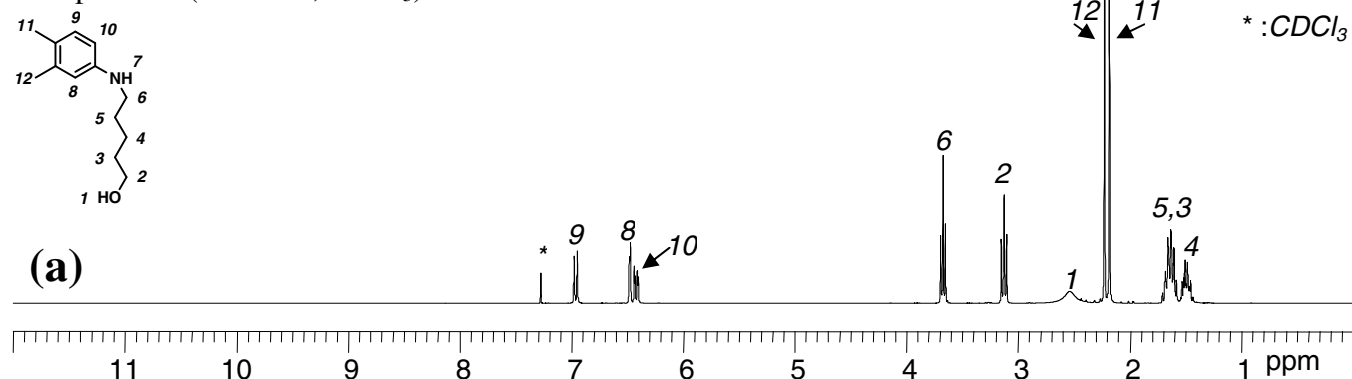


Compound **6** (400 MHz, DMSO-$d_6$)

Compound **7** (400 MHz, DMSO-$d_6$)

* : water
* : DMSO

(c)

Compound **8** (400 MHz, DMSO-$d_6$)

* : water
* : DMSO
* : ethanol

(d)

Compound **9** (400 MHz, DMSO-$d_6$)

* : water
* : DMSO
* : pyridine
* : ethanol

(e)
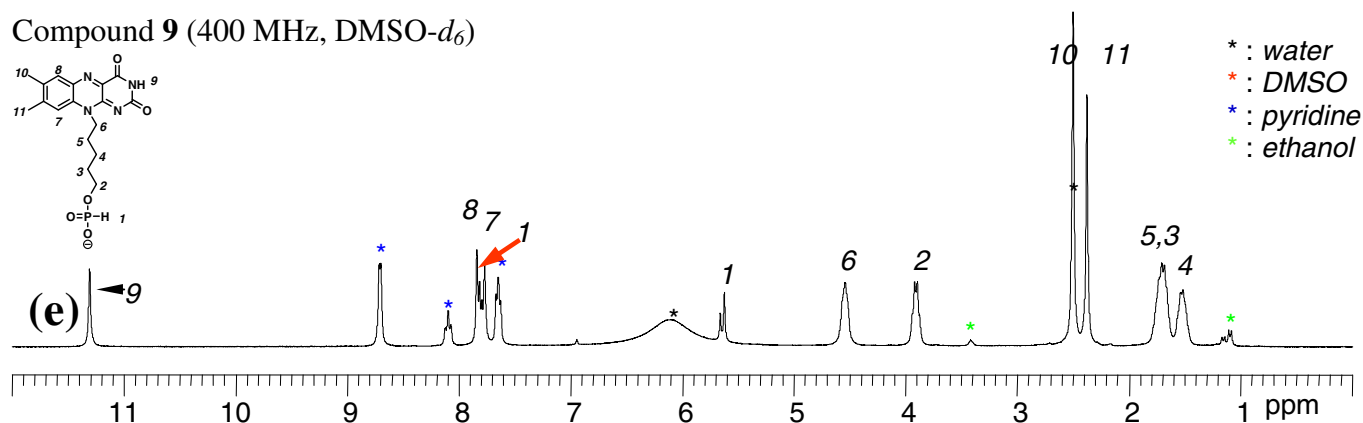
Compound **10** (300 MHz, DMSO-$d_6$)

* : water
* : DMSO
* : MeOH

(f)
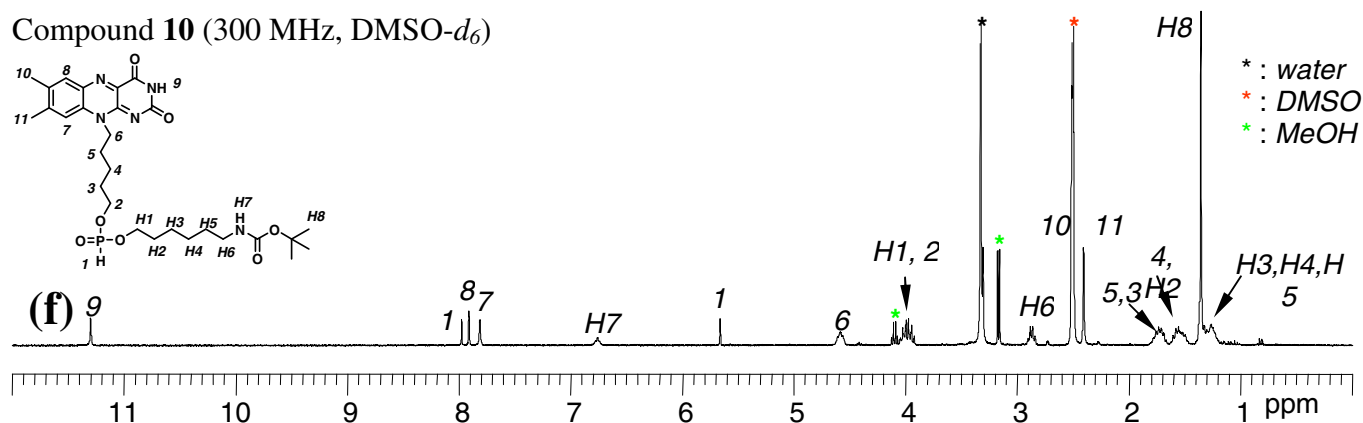
Compound **11** (300 MHz, DMSO-$d_6$)



**(g)**

* : water
* : DMSO
* : ethanol
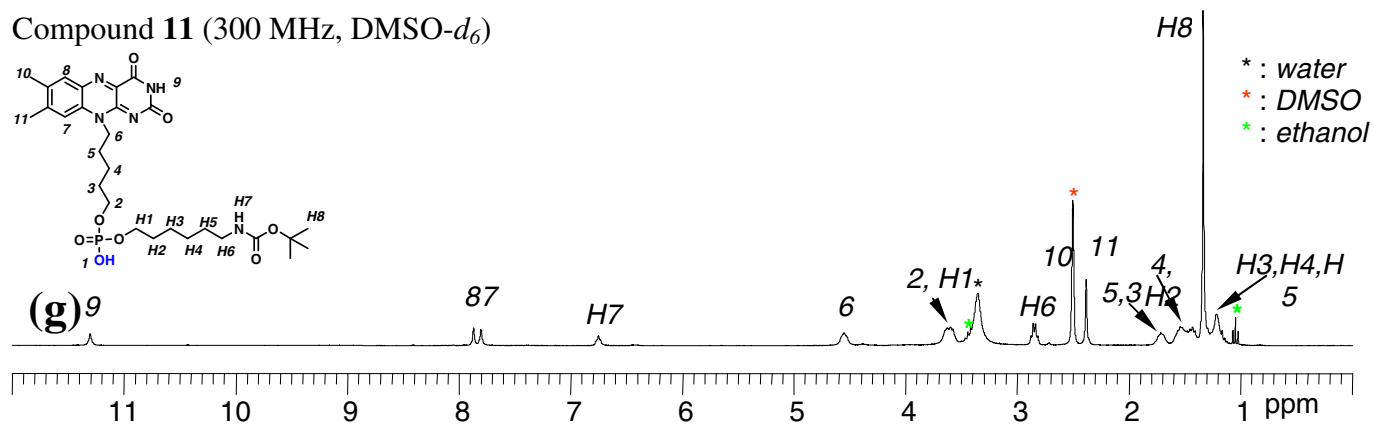
Compound **12** (300 MHz, D₂O)



**(h)**

* : water
* : ethanol

**HHCar** (300 MHz, DMSO-$d_6$)



**(i)**

* : water
* : DMSO
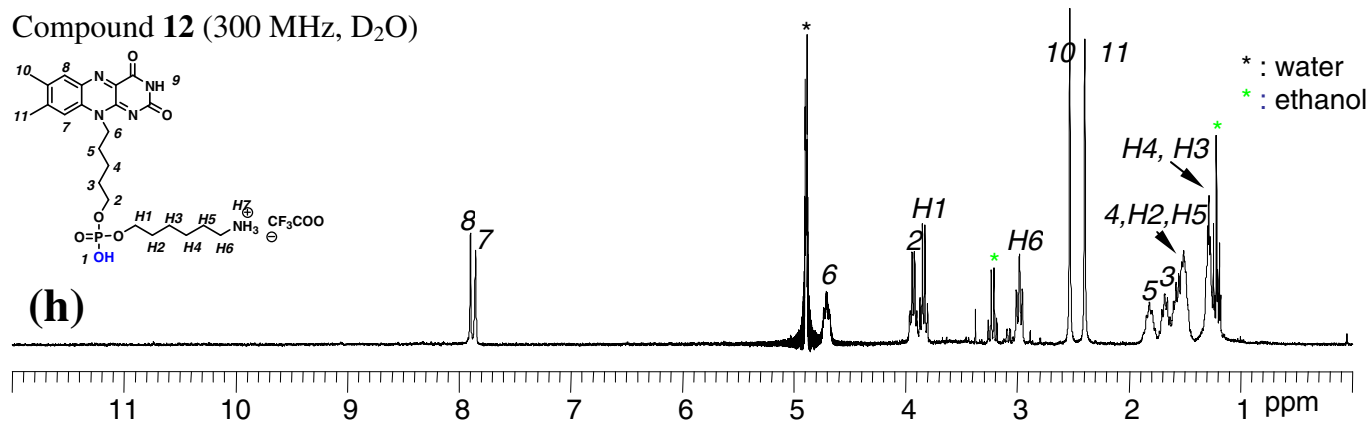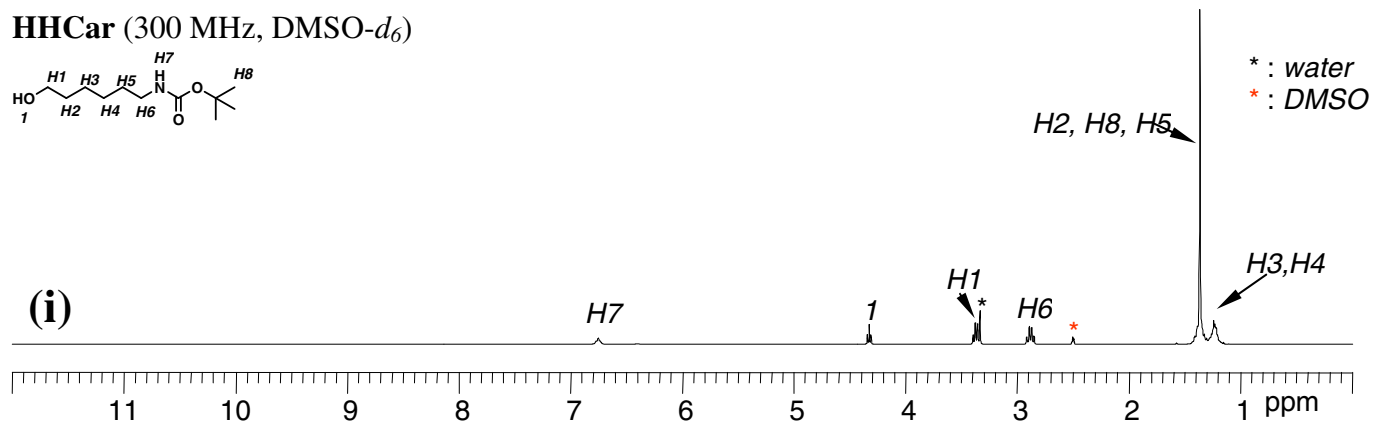
After coupling of **12** to **a-SWNT**, the **12-SWNT** product was subjected to four sonication-centrifugation-decantation (SCD) cycles for removing the unreacted **12** that might have been physisorped onto the nanotubes. Figure S2(a&b) illustrate the $^1$H NMR of **12** and **12-SWNT** (after 4 SCD cycles), respectively. The main peak (c.a. 5 ppm) in Figure S2b is due to $H_2O$. While no peaks in the aromatic region are observed, one can discern two broad peaks (c.a. 3.5 and 1.5 ppm). These peaks are currently believed to originate from the covalently attached **12**, whose lack of tumbling mobility due to the presence of the attached nanotube broaden their chemical shift. In order to remove any unreacted/physisorbed **12**, per-deuterated SDS-$d_{25}$ (98%) was added in the NMR solution of Figure S2b and sonicated further to promote surfactant-assisted detachment. Figure S2c illustrates the $^1$H NMR of SDS-$d_{25}$/**12-SWNT**. Aside from the presence of aliphatic protons (due to SDS-$d_{25}$ (98%)), no signal was observed in the aromatic region, even after considerable magnification (see inset). This indicates that the 4 SCD cycles successfully remove any unreacted/physisorbed **12** from **12-SWNT**.

**Figure S2**.     $^1$H NMR spectra of (a) **12**, (b) **12-SWNT** after four sonication-centrifugation-decantation (SCD) cycles to remove unreacted/physisorbed **12**, and (c) Fig. S2b solution sonicated with per-deuterated SDS-$d_{25}$ (98%). Inset illustrates the magnified aromatic region of Figure S2c.
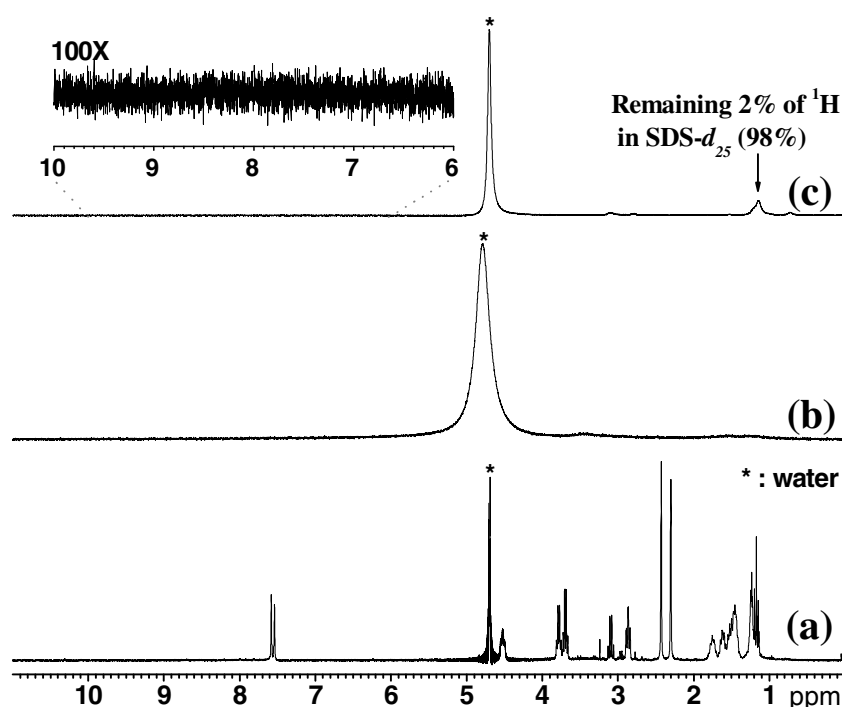
**Figure S3.** UV-Vis (right) and PL(left) spectra of synthesized flavin derivatives **8 – 12** ($10^{-4}$ M in water, except compound **10**, which was solubilized in EtOH). Excitation wavelength was 350 nm. All PL spectra were normalized at their intensity maxima.
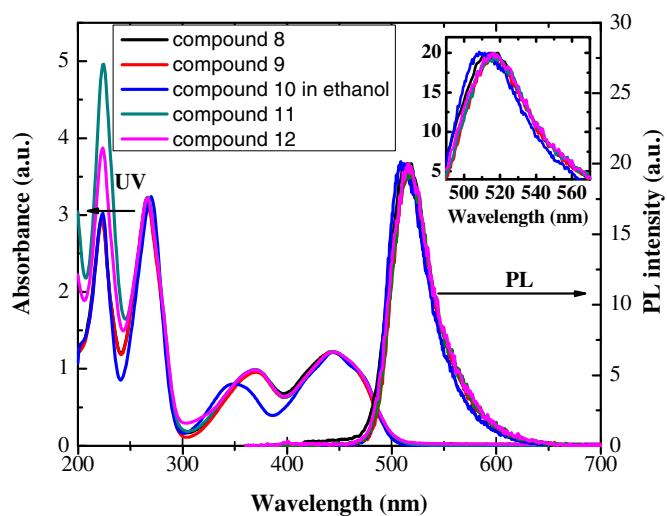
**Figure S4**. (a) UV-Vis (left) and PL (right) spectra of **12-SWNT** (flavin concentration : $5.8 \times 10^{-7}$ M) (trace 1) upon sequential sodium dithionite reduction (trace 2, $9 \times 10^{-6}$ M $Na_2S_2O_4$ was added) and air ($O_2$) re-oxidation (trace 3, $2.8 \times 10^{-5}$ M $O_2$ and trace 4, $1.4 \times 10^{-4}$ M $O_2$ were added), respectively. (b) SDS was added in trace 3 and 4. Excitation wavelength was 350 nm.

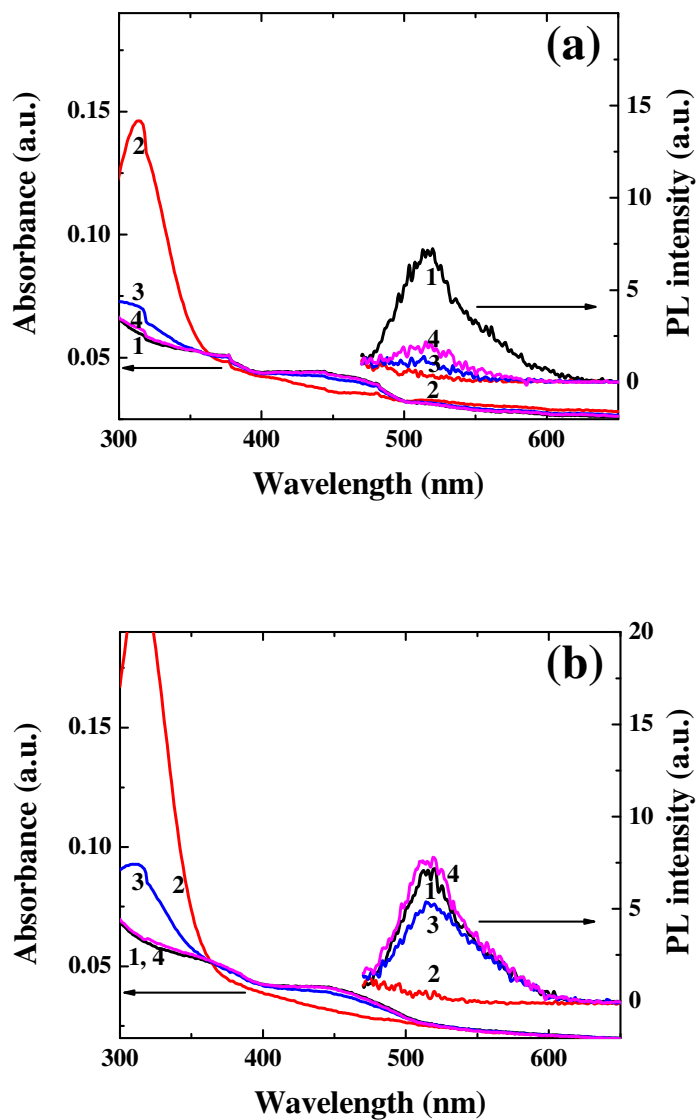**Figure S5**. Cyclic voltamogram of **8**, physisorbed onto SWNT forest electrode in PBS solution. Scan rate was 50 mV/sec.